THE JOURNAL OF PHYSICAL CHEMISTRY A

pubs.acs.org/JPCA Article

A Machine Learning Approach for Rate Constants. II. Clustering, Training, and Predictions for the O(^{3}P) + HCl → OH + Cl Reaction

Published as part of The Journal of Physical Chemistry virtual special issue "Machine Learning in Physical Chemistry".

Apurba Nandi, Joel M. Bowman,* and Paul Houston*

Cite This: *J. Phys. Chem. A* 2020, 124, 5746–5755 Read Online

ACCESS | Metrics & More | Article Recommendations

ABSTRACT: Following up on our recent paper, which reported a machine learning approach to train on and predict thermal rate constants over a large temperature range, we present new results by using clustering and new Gaussian process regression on each cluster. Each cluster is defined by the magnitude of the correction to the Eckart transmission coefficient. Instead of the usual protocol of training and testing, which is a challenge for present small database of exact rate constants, training is done on the full data set for each cluster. Testing is done by inputing hundreds of random values of the descriptors (within reasonable bounds). The new training strategy is applied to predict the rate constants of the O(^{3}P) + HCl reaction on the ^{3}A′ and ^{3}A″ potential energy surfaces. This reaction was recently focused on as a "stress test" for the ring polymer molecular dynamics method. Finally, this reaction is added to the databases and training is done with this addition. The freely available database and new Python software that evaluates the correction to the Eckart transmission coefficient for any reaction are briefly described.

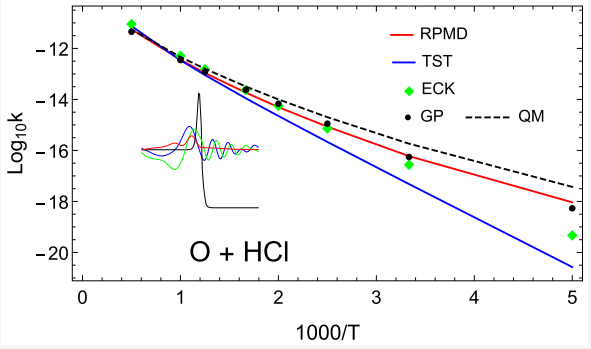

INTRODUCTION

The magic of chemistry lies in its methods for transforming one substance into another, but unless the conditions and speed for the transformation are favorable, the magic not only fails to awe but also loses its utility. Thus, the rates of chemical reactions and how they depend on conditions have long been the object of study. As early as 1889, Arrhenius discovered that the rates of chemical reactions vary as $A \times \exp(-E_a/T)$, where A is a constant, T is the Kelvin temperature, and E_a is the activation energy. A major subsequent advance came from the development of transition state theory (TST), which associated the activation energy with the location of a dividing surface that separated the reactants from the products in the space of energy versus configuration. For reactions that have a saddle point between reactants and products, the surface typically includes the saddle point. The constant A is associated in TST with a ratio of partition functions.

Both the Arrhenius equation and TST predict a near-linear relationship between the log of the rate constant with $(1/T)$. However, it soon became clear that for many reactions, quantum mechanical tunneling, not accounted for in TST, was a major perturbation at low temperatures, causing an increase in the rate constant from the linear prediction. Tunneling has since become a central focus of corrections to TST. The first proposals for incorporating tunneling effects into theory were based on one-dimensional potentials. Eckart's early work[1] is of particular relevance to what follows in this paper. This correction continues to be used,[2−4] primarily because it gives an analytical result that is often fairly accurate.

Other quantum mechanical (QM) approaches to the tunneling problem have also been developed. Most are computationally demanding and assume that a full potential energy surface (PES) for the reaction exists (such surfaces are themselves computationally demanding). For the most part, these new QM approaches have been applied to collinear reactions. An important compilation of such studies has been assembled by Allison and Truhlar.[5] A few three-dimensional calculations have also been reported, notably for the H + H_2 reaction.[6] These studies have shown the shortcomings of the one-dimensional Eckart model, including corner cutting tunneling paths, vibrationally adiabatic effects, recrossing of the TST dividing surface, etc. More recently, sophisticated QM

Received: May 14, 2020
Revised: June 12, 2020
Published: June 16, 2020

https://dx.doi.org/10.1021/acs.jpca.0c04348
J. Phys. Chem. A 2020, 124, 5746–5755

approaches have been developed to incorporate these effects, if only approximately. They include reduced-dimensionality quantum methods,[7−11] a large-curvature, corner-cutting reaction path,[5,12] instanton methods,[13,14] VPT2-based semiclassical transition state theory,[4,15−19] ring polymer molecular dynamics (RPMD),[20,21] and ring polymer instanton methods.[22] Exact direct methods to obtain the rate constant[23] have been implemented using multiconfiguration time-dependent Hartree (MCTDH) theory, at least for zero total angular momentum,[24,25] and then combined with *J*-shifting[9] to get the full rate constant.

These methods are improvements over the Eckart correction to conventional TST. However, none is exact. Numerous tests of them indicate a level of accuracy of about a factor of 1.5−2 for the rate constant at low temperatures. For example, for H + H_2, OH + H_2, and H + CH_4, this accuracy was reported for the RPMD method compared to benchmark results.[21,26−28] A very recent "stress test" of RPMD was reported for the O(^{3}P) + HCl reaction (on ^{3}A′ and ^{3}A″ potentials).[29] More discussion of this reaction will be given below.

We have previously reported a machine learning (ML) approach to train and predict bimolecular thermal rate constants over a large temperature range.[30] The reason for taking such an approach is the realization that the sophisticated approximate methods offer only a modest improvement over ECK-corrected TST results, except perhaps at very low temperature, at a cost of substantially more computational effort. The idea of our previous paper was to use ML to train a multiplicative correction to κ_{ECK} (see below for more details). We used exact quantum rate constants for mostly collinear (two-dimensional) reactions to determine the exact correction factor κ_{ECK}. Training was done with Gaussian process (GP) regression using a database of rate constants, usually at 8 different temperatures, for 13 reaction/potential surface combinations. Testing was performed on a set of 39 reaction/potential surface combinations. Averaged over all test reactions, the GP method was within 80% of the accurate answer, whereas transition state theory (TST) was only within 330% and Eckart corrected TST (ECK) was within 110%. The test reactions included 5 one-dimensional symmetric A + BA reaction/surface combinations; 16 one-dimensional asymmetric A + BC reaction/surface combinations; 15 three-dimensional reaction/surface combinations, both symmetric and asymmetric; and three polyatomic reactions: O + CH_4, H + CH_4, and HH + OH.

In this paper, we revisit this data set and employ a different training strategy; namely, in contrast to the earlier work, we train on the entire data set, which we divide into two clusters. We also examine one-dimensional correlations between χ and κ_{ECK} and also between χ and one descriptor we introduced in that paper (denoted u^*) and also κ_{ECK} itself. While these provide rough correlations, they are not sufficiently well correlated to use in quantitative work; i.e. there is a lot of scatter. With this in mind (and now after the fact) we return to the multidescriptor GP approach to train the entire data set. Testing is done by creating random trials of inputs to determine if the outputs are reasonable (to be defined below). We then apply the fully GP-trained χ to the new reaction O(^{3}P) + HCl.

In the next section, we briefly summarize the computational approach we use. We then present new predictions using the split data set to predict the rate constants for the O(^{3}P)+HCl reaction on the ^{3}A′ and ^{3}A″ potential energy surfaces. We perform a final training of data using results from that reaction and then describe how we make the new training data set and associated software, written in Python, freely accessible. A brief summary and conclusions are given in the final section.

COMPUTATIONAL APPROACH

The specific approach we proposed[30] is summarized next. Let $k(T)$ be an exact rate constant calculated over a temperature range and using a given PES, and let $k^{TST}(T)$ be the conventional TST rate constant using the same PES. The approach we took earlier is to represent the exact rate constant by the equation

$$k(T) = [\kappa_{ECK}(T)k^{TST}(T)]\chi(T) \quad (1)$$

where $\kappa_{ECK}(T)$ is the Eckart transmission coefficient[2,3,31] and $\chi(T)$ is the correction to the Eckart correction to produce agreement with the accurate rate constant. We reasoned that this approach is better than using ML on the exact $\kappa(T)$ directly because $\kappa_{ECK}(T)$ is easy to obtain and generally it does give realistic tunneling corrections. Thus, the hope is that the correction to the Eckart transmission coefficient is small and easy to "learn". To proceed with machine learning of $\chi(T)$ we need the usual three elements, namely a *database* of exact rate constants, a set of *descriptors*, and a general *machine learning method*, to train on the database. We described these in detail previously,[30] so we just briefly summarize these key elements here.

The descriptors are the parameters that characterize a reaction and of course their choice is critical for the success of the ML approach. For simplicity we first chose the three parameters that are needed to obtain the Eckart transmission coefficient.[2] In reduced units these are[30]

$$\alpha_1 = V_1/\omega_{im} \quad (2)$$

$$\alpha_2 = V_2/\omega_{im} \quad (3)$$

$$u^*(T) = \omega_{im}/(0.69307T) \quad (4)$$

V_1 (V_2) is the saddle point barrier height in cm^{-1} relative to the reactants (products), omitting the zero-point energy in both cases, and where the energy of the reactants is zero. ω_{im} is the magnitude of saddle point imaginary frequency (in cm^{-1}), 0.69307 is an energy conversion factor, $k_B/(hc)$, and T is the temperature in Kelvin. Modest improvements were obtained by including an additional parameter, the skew angle, β, which identifies important mass and corner cutting and recrossing effects. More details of these can be found in our recent paper.[30]

It turns out that training on the entire data set of roughly 400 values of χ is problematic because χ ranges from roughly 0.2 to 25 and thus it is a challenge to obtain high precision in fitting the entire χ data set. Thus, we decided to split the data into two clusters in a manner that would permit precise GP training on each. After some experimentation and visualization (see below), we split the data set at χ equal to 3.0. The cluster with χ greater than 3.0 is denoted the large-χ and the other cluster is denoted small-χ. This choice of boundary will become clear from several plots below which examine correlations of χ with κ and then with u^*

First, consider the correlation of χ with the κ_{ECK}, which hereafter we simply denote as κ. This is shown in Figure 1. As seen, there is a dense cluster of χ values in the lower left corner where κ is roughly one. These data typically correspond to the

https://dx.doi.org/10.1021/acs.jpca.0c04348
J. Phys. Chem. A 2020, 124, 5746−5755

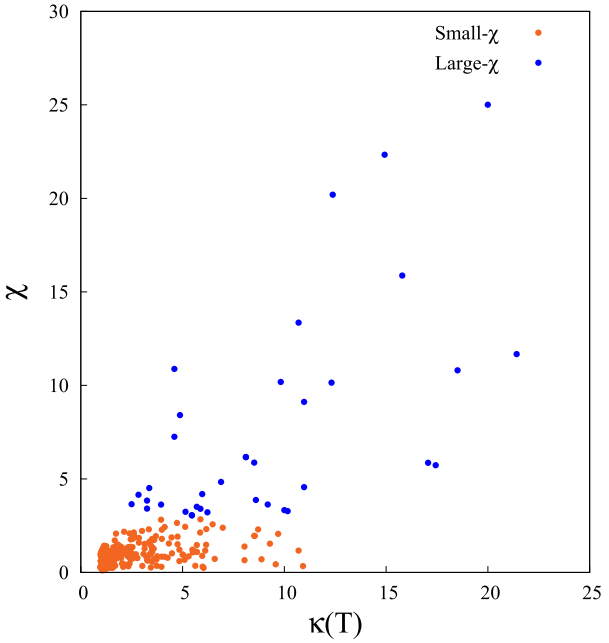

Figure 1. Plot of exact-χ versus Eckart κ for the entire data set but color coded according to the clusters described in the text.

high temperature regime where tunneling is not significant and where TST is fairly accurate but typically overestimates the exact $k(T)$. Thus, the χ-corrections to κ must be less than one, and as seen many are. By contrast at temperatures where tunneling is important κ is in the range of 10−20. Experience informs us that the Eckart κ typically underestimates the exact tunneling, owing to multidimensional effects such as corner-cutting. Thus, in the tunneling regime the expectation is that χ is also larger than one and indeed that is seen in the figure. This set of large χ-values is sparse and this is just a consequence again of the typical temperature range considered in rate constant calculations, i.e., 200 to 2000 K. Furthermore, as is typical, rate constant calculations are reported at intervals of 100 K and so most of the reported results are not in the tunneling region. This accounts for the high density of points in the lower left corner of the plot and the sparse density in the upper right corner. This has important consequences for our GP training, which we discuss below. In any case, there is good qualitative correlation between χ and κ. However, it is also clear that trying a simple 1d-regression analysis using κ would not produce useful quantitative results.

This figure also shows visually the rationale for choosing the boundary between the two χ-clusters at χ = 3.0. Of course this is not a unique choice. It is clear that this choice results in a small and sparse set of data for the large-χ cluster and clearly choosing a higher value would result in an even smaller cluster size. Choosing a smaller value for the boundary, e.g., 2.0, would increase the size of the cluster but at the expense of lessening the importance of the few but important large values of χ.

Next, consider the correlation between $\chi(T)$ and u^*, the only descriptor that depends on temperature. This is shown in Figure 2. As seen, there is a qualitative correlation for each cluster separately. This is not surprising as large values of u^* generally correspond to the tunneling region. The plot shown does appear promising for a one-dimensional regression analysis for each cluster. However, for the important large-χ cluster using standard least-squares fitting we were unable to achieve a R^2 metric better than around 0.77.

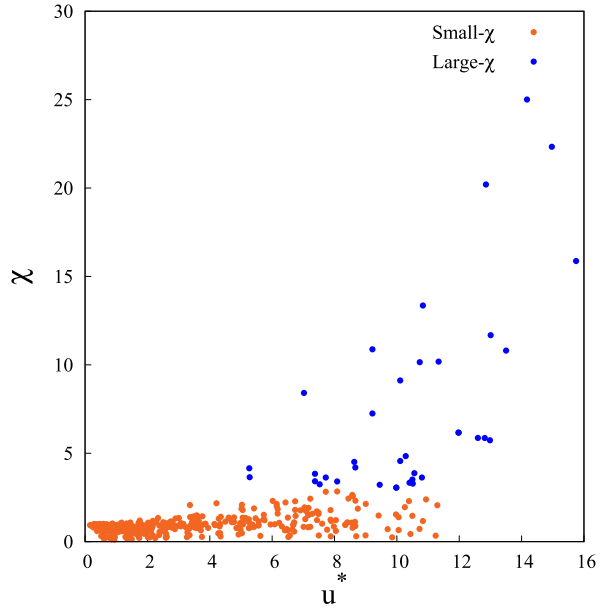

Figure 2. Exact χ versus u^* and for the entire χ data set.

Several features of this plot are important to note. First, there is a region of overlap between the two clusters for u^* in the range of around 6 to 12. Second, u^* values below 5 appear only in the small-χ cluster and finally u^* values above 12 appear only in the large-χ cluster. These features will be important for the new application to the $O(^3P)$ + HCl reaction.

As an aside, we note that the so-called crossover temperature is where u^* equals one. The reason for this terminology is that it is a indicator of temperature above which instanton theories may no longer apply.[22] Here it serves as a rough indicator of where tunneling is important, as seen directly in Figure 3. From this figure, we see that κ is not significantly larger than

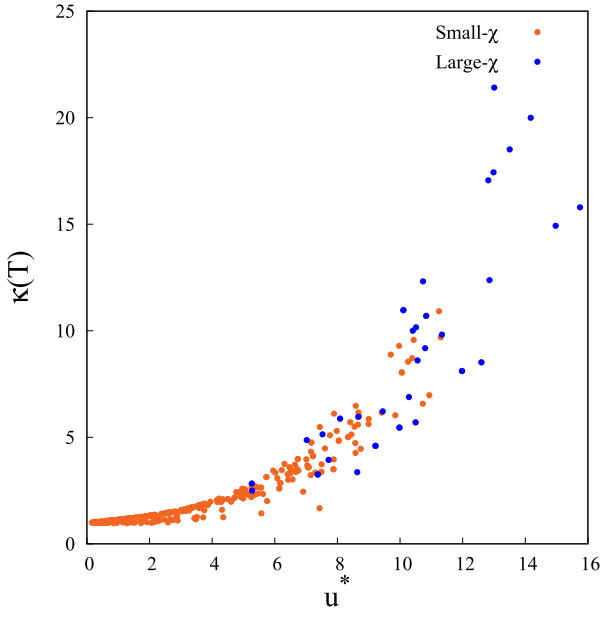

Figure 3. Eckart κ versus u^* for the entire data set.

https://dx.doi.org/10.1021/acs.jpca.0c04348
J. Phys. Chem. A 2020, 124, 5746−5755

one (indicating tunneling) for u^* less than one and that large values of κ, i.e., greater than 5, are seen for u^* greater than roughly 8.

Returning to the goal of representing the two χ clusters, we proceeded, as before,[30] with a more sophisticated regression method, namely GP, which we very briefly summarize next. This is a machine learning method that aims to produce a smooth interpolation between known data and to reproduce the data to within a specified uncertainty.[32] The working equation is given by

$$\chi(\boldsymbol{x}) = \mathbf{K}_x^{\mathrm{T}}\mathbf{K}^{-1}\boldsymbol{\chi}_0 \tag{5}$$

where $\boldsymbol{x}$ represents a set of variables, known as descriptors. The known values of χ are collected in the column vector denoted $\boldsymbol{\chi}_0$. $K(\boldsymbol{x}_i, \boldsymbol{x}_j)$ is the kernel matrix with elements at the database values of $\boldsymbol{x}$ and where $\mathbf{K}_x = [k(\boldsymbol{x}, \boldsymbol{x}_1) \cdots k(\boldsymbol{x}, \mathbf{x}_N)]^{\mathrm{T}}$. In this expression, $\boldsymbol{x}$ is the value of the descriptors where χ is to be evaluated. A popular choice for the kernel matrix is[32−34]

$$K(\boldsymbol{x}_i, \boldsymbol{x}_j) = \sigma^2 \exp\left(-\frac{d_{ij}^2}{2}\right) + \delta_{ij}\sigma_{noise} \tag{6}$$

where d_{ij} is the distance between the two vectors $\boldsymbol{x}_i/l$ and $\boldsymbol{x}_j/l$, where the hyper-parameters are l and σ. The length-scale parameter can be single length or one that depends on the descriptor; we use the latter. $\delta_{ij}\sigma_{noise}$ is the noise term that is added to the diagonal of the covariance matrix. In principle, this term is not necessary for fitting, because the data are not noisy. However, adding noise can avoid ill-conditioning of the matrix and this generally enters parametrically into the optimization of the hyper-parameters according to maximization of log-marginal-likelihood.[32,35]

$$\log \mathcal{L} = -\frac{1}{2}(\mathbf{g}^{\mathrm{T}}\mathbf{K}^{-1}\mathbf{g} + \log|\mathbf{K}| + N \log 2\pi) \tag{7}$$

Once the optimal hyper-parameters are determined, the GP model can predict the value of χ using eq 5. In a practical sense, the hyper-parameters govern the smoothness of the interpolation, also known as prediction. We return to this important point later.

We performed this GP regression on the small- and large-χ data sets using the routines contained in the Python scikitlearn library, which includes optimization of the hyperparamters.[36] The inputs are the descriptors and the output is the trained χ. We developed the database for exact χ largely from a 1998 compilation of rate constants[5] as well as results from several more recent quantum calculations of rate constants for polyatomic reactions, such as OH + H_2, H + CH_4, and O + CH_4, as described in detail previously.[30]

Fitting Results. The small-χ data set has a total 360 data points, and we took all the points to fit the data set using GP regression. The RMS error of this fitting is 0.14461. This fitting result is shown in Figure 4. As seen, there is very good correspondence, with a handful of minor outliers. As we use all the data points to train, we decided to test this fit on several hundreds of random inputs where this random inputs are within the range of each descriptors for this cluster. The purpose of this is to examine the quality of the predictions. The details of this random stress test results using small-χ cluster are given in the next section.

The large-χ data set has total 37 data points, which for ML is very small. Given this small training number, overfitting is a well-known issue in ML for the data points that are far from training data points and also can get prediction with large uncertainty. In regard of this, we investigated training using two different "noise" values, one 0.0001 and the other is 0.4. As expected for the former small noise value the RMS error of the fitting is 0.67895 and the maximum likelihood is −949.240. This fitting result is shown in Figure 5. As expected the training is precise. However, it turns out that this precise fitting is actually overfitting. When we use this fit to test on hundred random inputs, 70% of this data predicts χ outside of its range with large uncertainty.

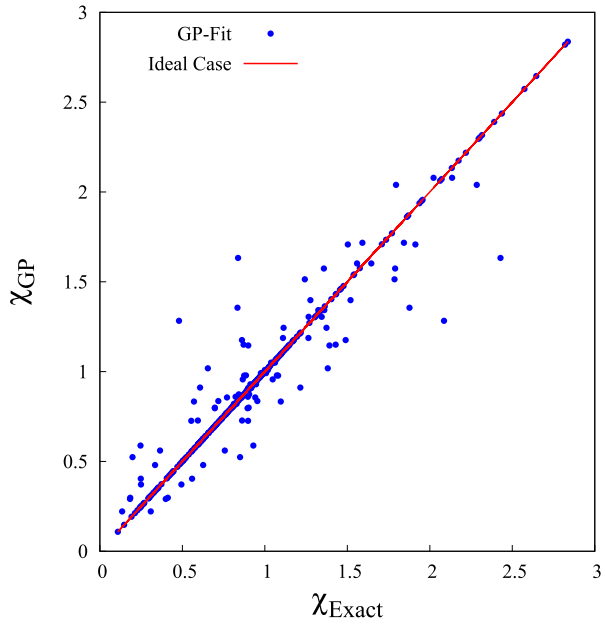

Figure 4. Trained-χ versus exact-χ for the small-χ data set.

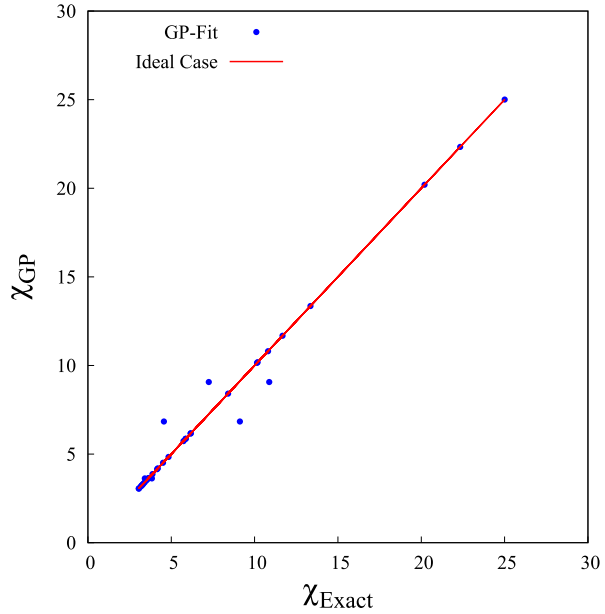

Figure 5. Trained-χ versus exact-χ for the large-χ data set with σ_{noise} = 0.0001.

Next we decided to use large noise value to overcome this overfitting and hopefully to get a much more stable prediction. The second training, using the larger noise value leads to an

https://dx.doi.org/10.1021/acs.jpca.0c04348
J. Phys. Chem. A 2020, 124, 5746−5755

RMS fitting error of 3.6, with max. likelihood = −108.318. This fitting result is shown in Figure 6. When we use this fit to test

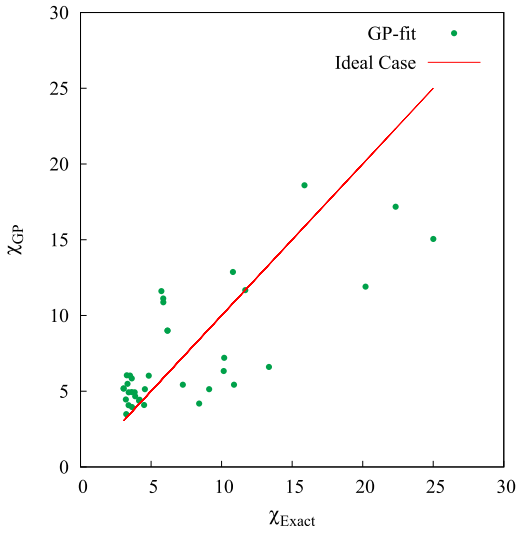

Figure 6. Trained-χ versus exact-χ for the large-χ data set with σ_{noise} = 0.4.

on those hundred random data, only for 10% of this data predicts χ below 3. The details of this random stress test results using large-χ cluster are given in the next section. By using large noise values we lose some precision for training data but this makes more coarse approximations which avoids over fitting to noisy data. Virtually any prediction using these fits will not be substantially affected by these outliers given that there are only factors of 2 or so different from the exact results. Finally, two points are worth making about this training. One is that closer agreement between the trained and exact data could be achieved by using much smaller values of σ_{noise}, assuming the matrix inverse is not singular. However, experiments doing this verify that this leads to the GP version of overfitting, which results in unstable predictions. The second point is that training on the full data set of exact χ leads to significantly worse results for large values of χ than training on the two clusters of χ.

The conventional approach to verify the robustness of the training is to then test on a part of the data not included in the training. This can be done for the small-χ cluster since it contains 360 data points. Here we decided to take 10 or 20% of data for testing purpose from small-χ cluster. So, we randomly chose 10 or 20% small-χ cluster data for testing purpose and remaining 90 or 80% data for training purpose. The performance of GP on both the training and testing data are very good and consistent. The RMS errors for these 90% and 80% training data are 0.14459 and 0.14460; and RMS error for 10% and 20% test data are 0.1346 and 0.1277 respectively. These fitting results are shown in Figure 7. Unfortunately, we can not follow this strategy for large-χ cluster because of its small number of data. So, we propose another way to test the training on this cluster by using random inputs and investigating the quality of the predictions. This is presented below. For completeness and comparison we also perform this test for the training on the small-χ cluster.

Stress Testing χ_{GP} Predictions. In the absence of additional data to test on, we decided to use the trained GP with hundreds of random inputs. The goal is to examine and assess the quality of the predictions qualitatively and semiquantitatively. This is done for each cluster and selecting values of the descriptors within the range of each descriptor for each cluster. We generated inputs by a random selection of each parameter within their range for each cluster to predict the χ value from GP fits. The ranges of these parameters for each cluster are as follows: for the large-χ data set the ranges are as follows: u^*, 5.27−15.75; α_1, 1.46−3.51; α_2, 1.46−6.24; and β, 13.6−89.3°. For the small-χ data set: u^*, 0.16−12.56; α_1, 1.03−3.51; α_2, 0.71− 95.12; and β, 11.6−89.3°. These are large ranges, so the four-dimensional volume enclosed by them is very large compared to cluster data set sizes of 37 and 360, respectively.

We generated 400 random (uniform) inputs for the prediction of χ from the small-χ fitting cluster and 100 points for the prediction of χ from large-χ fitting cluster. The GP prediction results are predominantly satisfactory in the sense

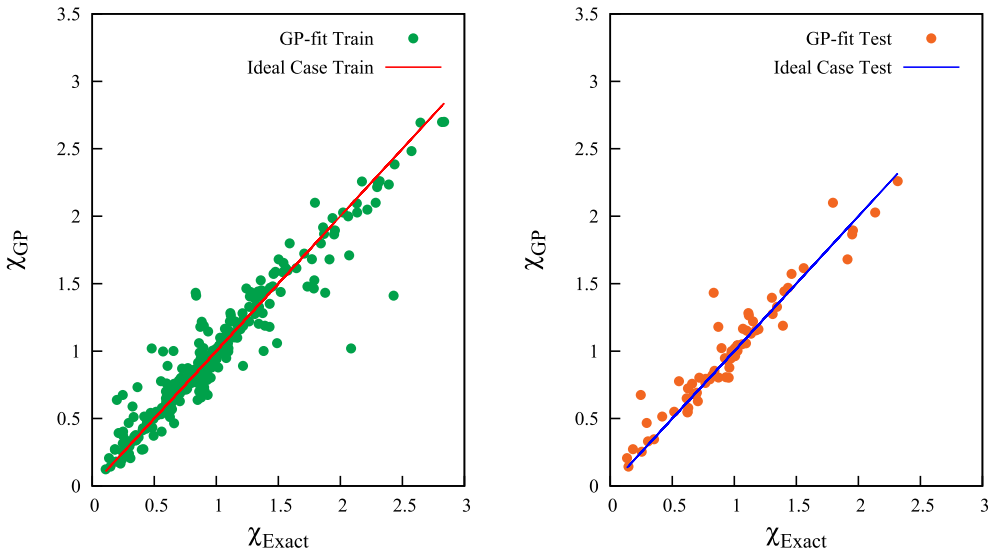

Figure 7. Trained-χ versus exact-χ (left panel) where the 80% data of the small-χ cluster is used for training, and test-χ versus exact-χ (right panel) where the remaining 20% data of the small-χ cluster is used for predictions.

https://dx.doi.org/10.1021/acs.jpca.0c04348
J. Phys. Chem. A 2020, 124, 5746−5755

that they are in the range of a few tenths to 3 for small-χ cluster and 3 to 25 for the large-χ cluster. These results are shown in Figure 8. However, as expected, we found some predicted χ values at zero and negative values. This is a well-known issue in GP (and all nonparametric ML methods) that if the input is "far" from training values we can get unexpected prediction from GP. Here we traced most poor predictions in the small-χ cluster due to the α_2 parameter. The values of the α_2 parameter have a very large range, from 0.71 to 95.12. However, from the nature of the training data most α_2 values lie between 0.71 and 10 and there are only six extremely exothermic reactions where α_2 values are 34.11, 58.17, 64.31, 73.78, 87.05, and 95.12 respectively. Thus, the values of the α_2 parameters are highly scattered between the range from 10 to 95 for the small-χ cluster, causing unexpected predictions. Similarly, we get poor predictions (zero and negative values) from the large-χ cluster specially when we use very small noise value to fit the data. 70% of this data predicts the χ value outside the range with high uncertainty between 3 and 10.

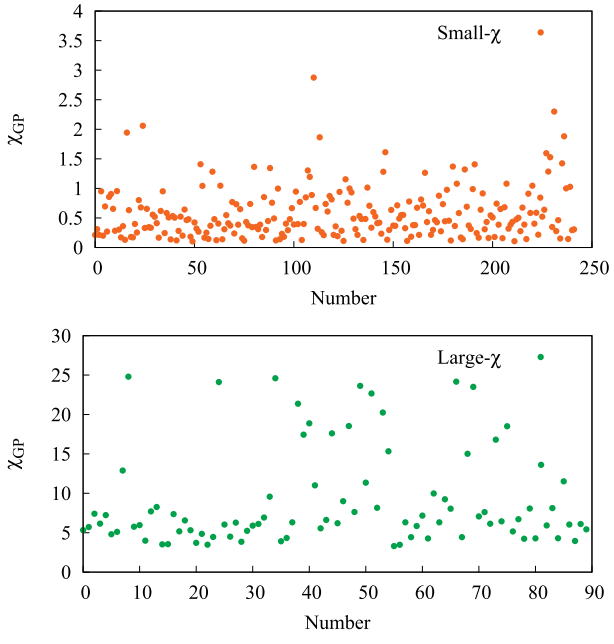

Figure 8. Random stress test: Predicted-χ from both small-χ and large-χ.

This bad performance is due to the overfitting. When we use a larger noise value, σ_{noise} = 0.4, we get much better results. Here, 90% of this data predicts the χ value between 3 to 25 with uncertainties, between 3 and 5.5. In this case most of these are traced to highly scattered distribution of β within that range. However, we found no predictions for χ greater than 25.0 because for large-χ cluster the χ values are ranging from 3.0 to 25.0, which is expected from the GP. The GP prediction results for these stress tests are shown in Figure 8.

Overall, we conclude that the GP regressions trained on the two clusters perform satisfactorily for predictions. However, we do not have a quantitative assessment of this performance. The next section provides one assessment with an application to a challenging chemical reaction not included in the training data.

$O(^3P) + HCl \rightarrow OH + Cl$ Reaction. This H atom transfer reaction is of central importance to chemical kinetics. One reason is that it can take place on $^3A'$ and $^3A''$ potentials, both of which are known to have large barriers to reaction. Another is that it is an example of a heavy-light-heavy reaction, which presents additional challenges to transition state theory owing to possible enhanced tunneling at low temperatures and substantial recrossing at high temperatures. And with the availability of extensive experimental data spanning a large temperature range, the extensive theoretical modeling of this reaction is understandable.[29,37−45] The most recent work has made use of high-level *ab initio* PESs for both electronic states in three-dimensions with essentially exact quantum calculations of the rate constants.[45] These PESs were also used in a recent "stress test" of RPMD.[29]

Before presenting predicted rate constants, we give the four descriptors, the Eckart transmission coefficient and the predicted χ as a function of temperature for the $^3A'$ and $^3A''$ PESs in Tables 1 and 2, respectively. The values of α_1 and α_2 for both PESs are well within the ranges of these descriptors for both χ clusters. The skew angle β is close to the smallest value in each cluster. The temperature-dependent descriptor u^* value of 15.45 at 200 K for the $^3A'$ PES is close to the upper limit of that descriptor in the training data for the large-χ cluster. The corresponding u^* for the $^3A''$ PES equals 13.28. As seen in Figures 2 and 3 these values of u^* appear only in the large-χ cluster and so the predicted χs, 17.1 and 11.5, come from the training using the large-χ cluster. This training was done with the noise value of 0.4. We defer further discussion of this training to the next section.

For temperatures above 600 K for the $^3A'$ PES and for temperatures above 500 K for the $^3A''$ PES, the u^* values appear only in the small-χ cluster, and so predictions come from training on that cluster. For temperatures between these and 200 K, u^* appears in both clusters. However, because there is far more data in the small-χ cluster we take predictions from the training on that cluster. We return to the choice of

Table 1. Descriptors, Eckart Transmission Coefficient κ, and χ_{GP} for the $O(^3P)$ + HCl Reaction, for the $^3A'$ PES

PES $^3A'$						
T (K)	u^*	α_1	α_2	β (deg)	κ	χ_{GP}
200	15.45623	2.24797	2.34592	17.0	40.65620	17.1409472[a]
300	10.30415	2.24797	2.34592	17.0	9.27109	1.6296824[b]
400	7.72811	2.24797	2.34592	17.0	4.68260	1.3960705[b]
500	6.18249	2.24797	2.34592	17.0	3.19085	1.2837793[b]
600	5.15208	2.24797	2.34592	17.0	2.50587	1.1786288[b]
800	3.86406	2.24797	2.34592	17.0	1.88932	1.0168079[b]
1000	3.09125	2.24797	2.34592	17.0	1.61526	0.9174855[b]
2000	1.54562	2.24797	2.34592	17.0	1.22566	0.7512409[b]

[a]Predicted from the large-χ data set. [b]Predicted from the small-χ data set.

https://dx.doi.org/10.1021/acs.jpca.0c04348
J. Phys. Chem. A 2020, 124, 5746−5755

Table 2. Descriptors, Eckart Transmission Coefficient κ, and χ_{GP} for the O(^{3}P) + HCl Reaction, for the ^{3}A″ PES

PES ^{3}A″						
T (K)	u^*	α_1	α_2	β	κ	χ_{GP}
200	13.2791	2.01417	2.12818	17.0	17.4824	11.5288124[a]
300	8.8527	2.01417	2.12818	17.0	5.68433	2.0346086[b]
400	6.6395	2.01417	2.12818	17.0	3.37346	1.5307440[b]
500	5.3116	2.01417	2.12818	17.0	2.51248	1.2014101[b]
600	4.4264	2.01417	2.12818	17.0	2.08464	1.0029277[b]
800	3.3198	2.01417	2.12818	17.0	1.67331	0.7817502[b]
1000	2.6558	2.01417	2.12818	17.0	1.47946	0.6600456[b]
2000	1.3279	2.01417	2.12818	17.0	1.18664	0.4315121[b]

[a]Predicted from the large-χ data set. [b]Predicted from the small-χ data set.

Table 3. Rate Constants (cm^3/(mol-s) for O(^{3}P) + HCl → OH+Cl from Indicated Methods and Potential Energy Surface (PES)

	PES ^{3}A′			PES ^{3}A″		
T (K)	TST	GP	RPMD	TST	GP	RPMD
200	6.73×10^{-25}	4.69×10^{-22}	5.16×10^{-22}	2.67×10^{-21}	5.38×10^{-19}	9.22×10^{-19}
300	1.20×10^{-20}	1.81×10^{-19}	1.40×10^{-19}	4.78×10^{-18}	5.53×10^{-17}	5.97×10^{-17}
400	1.75×10^{-18}	1.14×10^{-17}	5.95×10^{-18}	2.14×10^{-16}	1.11×10^{-15}	8.49×10^{-16}
500	3.78×10^{-17}	1.55×10^{-16}	7.58×10^{-17}	2.20×10^{-15}	6.64×10^{-15}	4.91×10^{-15}
600	3.11×10^{-16}	9.18×10^{-16}	4.79×10^{-16}	1.08×10^{-14}	2.26×10^{-14}	1.81×10^{-14}
800	4.91×10^{-15}	9.43×10^{-15}	5.41×10^{-15}	8.53×10^{-14}	1.12×10^{-13}	1.03×10^{-13}
1000	2.86×10^{-14}	4.24×10^{-14}	2.63×10^{-14}	3.15×10^{-13}	3.08×10^{-13}	3.35×10^{-13}
2000	1.56×10^{-12}	1.44×10^{-12}	9.99×10^{-13}	5.97×10^{-12}	3.06×10^{-12}	4.58×10^{-12}

cluster in the case of overlapping descriptors in the next section. Finally, we note that at high temperatures χ_{GP} is less than one, which is a correction for recrossing, relative to the Eckart κ.

Table 3 contains the rate constants from TST, the predicted GP (recall that this is just the product of TST κ and χ), and RPMD for the A′ and A″ PESs. As seen TST is nearly 3 orders of magnitude below RPMD at 200 K and about a factor of 10 lower at 300 K. The GP results are in good agreement with RPMD over the entire temperature range, and of course notably at 200 K. At this temperature, χ is more than a factor of 10 and so a large correction to the Eckart transmission coefficient.

These rate constants are shown graphically in Figure 9 along with the summed rate constant plot, which includes the accurate quantum result. Note, all calculations use the same potential energy surfaces and only the summed QM results were given previously over the temperature range of the plot.[45] First, the nice agreement between GP and RPMD is shown in these plots. Second, as was noted earlier in the "stress test" of RPMD, the quantum summed rate constant is significantly larger than the RPMD (and GP) one. Note the quantum rate constant for the A′ surface was not reported. The origin of this enhanced quantum tunneling is low energy reactive resonances on the A″ PES due to van der Waals wells. This has been thoroughly discussed in the literature.[44,45] Resonances are not described by RPMD or other approximate methods. A heuristic method to account for resonance enhanced tunneling has been suggested.[47] From the perspective of the present ML approach this enhanced tunneling could be incorporated into the database of exact corrections to the Eckart transmission coefficient. We return to this point in the next section.

DISCUSSION

The goal of machine learning corrections, χ, to the widely used Eckart transmission coefficient relies on having a well-developed database of accurate rate constants. No such database existed before our first effort to establish one.[30] We used a combination of exact quantum calculations for collinear models of A + BC reactions, and a small number of accurate quantum calculations for polyatomic reactions in full dimensionality. The database does span a fairly diverse set of reactions and potential energy surfaces and rate constants that span a large temperature range. Numerically the largest corrections come at the lowest temperature in the database, 200 K. This is where tunneling is largest and where the Eckart transmission coefficient underestimates tunneling the most. Of course, there is relatively very little data at this temperature. It is difficult to add to the database, especially at low temperatures, since this requires a major computational effort starting with a potential energy surface and then an accurate calculation of the rate constant.

The strategy in this paper to deal with this sparse set of large χ values is to divide the database into small and large χ clusters using a boundary of χ = 3.0. As noted already, this results is a small data set for the large-χ cluster. Thus, the trade-off in training precision versus overfitting is especially important for this cluster. We could not follow the usual protocol of training and testing with this cluster owing to its small size. So, we opted to use random inputs for testing predictions and this led us to prefer training with a noise value of 0.4 over one with a much smaller value of 10^{-4}.

A demanding test of the strategy and training was done for the O(^{3}P) + HCl reaction. As noted in the recent literature,[29] the reaction was chosen as stress test for approximate methods owing to the large reaction barrier (on both PESs), small skew angle, and low-energy reactive resonances.[44,45] The results did

https://dx.doi.org/10.1021/acs.jpca.0c04348
J. Phys. Chem. A 2020, 124, 5746−5755

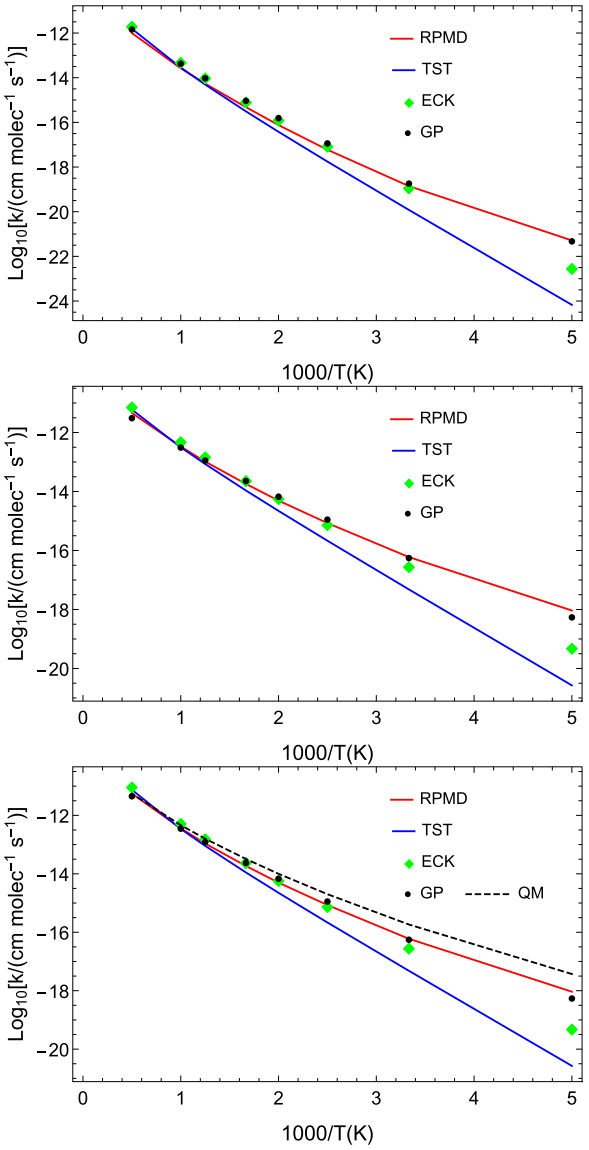

Figure 9. Comparison of rate constants for the O + HCl reaction (top) for the A′ surface, (middle) for the A″ surface, and (bottom) for the sum of the two. RMPD results are from ref 29, TST results are from ref 46, QM results are from ref 45, and ECK and GP results are from this work.

make use of GP training on both the small-χ and large-χ clusters, however, for the latter only at 200 K where tunneling is very large. For both PESs, the GP-corrected rate constants are less than a factor of 2 lower than the RPMD ones which are almost 10^3 larger than TST for both PESs. At this temperature, the χ values are 17.1 and 11.5 for the A' and A'' surfaces, respectively. These are large corrections to the Eckart transmission coefficients for these surfaces. While this an encouraging result for prediction using the large-χ cluster, it must be noted that the RPMD rate constant is a factor of 4, and thus, the GP one is roughly a factor of 8 below the accurate quantum rate constant at 200 K. At 300 K, both RPMD and GP are below the accurate rate constant by about a factor of 3 whereas TST is below by about a factor of 38. At higher temperatures all methods merge to a level of agreement within about a factor of 2.

It is worth noting that we did use the more precise large-χ training and used that training to get predicted values of χ at 200 K. They are 6.95 and 7.13 for $^3A'$ and $^3A''$ PESs, respectively. But these predictions came with large uncertainties of 8.25 and 5.90, respectively. These large uncertainties are the price paid for making the training overly precise on a small data set. The predicted χ values from the less precise but more robust training on the large-χ are 17.14 and 11.52. These come with smaller uncertainties of 4.6 and 4.2 for $^3A'$ and $^3A''$ PESs, respectively. Thus, the rate constant predictions at 200 K are probably uncertain to about 25−35%.

Overall the present GP training strategy was successfully applied to the demanding O(^{3}P)+HCl reaction. Looking ahead, the exact corrections to the Eckart transmission coefficient can be done for this reaction for both PESs. There is more data for the reactive $^3A''$ PES because the quantum rate constant was reported from 200 to 3000 K. For the higher-barrier $^3A'$ PES, useful data are available above roughly 600 K.[29,45] These will be included in a new data set that will be made readily available as described in detail in the next section.

We conclude this section with a suggestion for weighting the predictions of GP training on multiple clusters.

Weighting Clusters. Merging machine learning on different clusters (data sets) ultimately comes down to weighting the outputs. There are numerous ways to do this, e.g., switching functions and Shepard-type weights. The choice/invention of weighting is often problem-specific and thus not unique. For example, there are numerous functional forms for switching functions that vary from 0 to 1. However, in general the approaches rely on a distance metric that measures the distance of an arbitrary input relative to some point or points associated with each cluster.

Here the inputs are the four descriptors and since the clusters are small we use each point in each cluster from which to determine a distance. We simply copy the distance contained in the GP kernel matrix described in the Computational Details section. Thus, letting $[x_1, x_2, x_3, x_4]$ be the vector representing u^*, α_1, α_2, and β, then the distance of $\mathbf{x}$ from a data point in cluster j is given by

$$d_{i,j} = \sqrt{\sum_{m=1}^{4} \left(\frac{x_m - x_m(i,j)}{l_m(j)} \right)^2} \tag{8}$$

where $l_m(j)$ is the optimized length for each descriptor in cluster j. Then we define the weight of each point i in cluster j as the reciprocal of d_{ij} and thus the total weight for cluster j is given by

$$w(j) = \sum_{i=1}^{N_j} \frac{1}{d_{i,j}} \tag{9}$$

where N_j is the number of data in cluster j. Note this weight is not normalized and so normalized weights are given trivially by

$$W(j) = w(j) / \sum_{n=1}^{N} w(n) \tag{10}$$

where N is the number of clusters, This proposal for the weight of cluster has the following properties. First, if an input happens to matches the data in a cluster the (unnormalized) weight of that cluster is infinite, i.e., all other weights are zero, and thus the normalized weight of that cluster is 1 exactly, as it

https://dx.doi.org/10.1021/acs.jpca.0c04348
J. Phys. Chem. A 2020, 124, 5746−5755

should be. Second, by adding reciprocals the effect of the cluster size is greatly mitigated. That is because data that are relatively far removed from the input contribute negligibly to the total weight. This obviates the need for a data cutoff parameter.

To apply this proposal for cluster weights to the $O(^3P)$ + HCl reaction, we return to the case where the input is present in the large and small-χ clusters, namely when u^* = 10.30415, 7.72811, 8.8527, and 6.6395 (from Tables 1 and 2) for this reaction. We computed the weights for these inputs using the eqs 8−10. The maximum weight for the large-χ cluster is about 2% for u^* is 10.30415. For u^* less than 10, this weight for the large-χ cluster is less than 1%. So, in these cases, the contributions from the large-χ is negligible.

SOFTWARE

We have made the complete exact χ data set with the inclusion of new values from the O + HCl reaction as well as a Python code to perform GP training and prediction and several sample input and outputs for the present application available.[48] The software does print warnings if the inputs or the predictions are out of range of the training data for the small-χ and large-χ clusters.

SUMMARY AND CONCLUSIONS

We presented a strategy to correct the Eckart transmission coefficient using clustering and new Gaussian process regression on two clusters of exact corrections, χ. Each cluster is defined by the magnitude of the correction to the Eckart transmission coefficient. Instead of the usual protocol of training and testing, which is a challenge for the present small database of exact rate constants, training is done on the full data set for each cluster. Testing is done by inputing hundreds of random values of the descriptors (within reasonable bounds). The new training strategy was applied to predict the rate constants of the $O(^3P)$ + HCl reaction on the $^3A'$ and $^3A''$ potential energy surfaces. This reaction was recently focused on as a "stress test" for the ring polymer molecular dynamics method. The new GP predicted rate constant is in very good agreement with the RPMD ones over the entire temperature range and notably at 200 K, where standard TST is almost 3 orders of magnitude smaller. Exact corrections using accurate quantum calculations of the rate constant for this reaction are added to the database of corrections to the Eckart transmission coefficient. Details to access this updated database and new Python software that does GP training and prediction are given. We hope to make further tests of the current model and training databases as benchmark rate constants are reported. Such calculations are highly computationally demanding and so expanding the training database will be a slow process. Another possible expansion of the current model is to consider additional descriptors, for example one that identifies reactions, such as the present one, where low-energy resonances lead to enhanced tunneling.

Finally, a concluding opinion on ML that may apply generally. It is that ML is at heart an interpolation method that relies on reliable and extensive data to train on. What we might term trivial extrapolation may work, but extrapolation beyond what is learned by training the known data set is not possible. The $O(^3P)$ + HCl reaction is a good example of this. The enhanced tunneling due to low-energy resonances obviously cannot be learned from a database that does not contain examples of such reactions. So in a sense ML may be able to replace computationally intensive calculations for "routine" applications, where "routine" means applications that are learned from existing training. When ML fails, e.g., by producing a prediction in poor agreement with experiment, this is potentially good and significant news since it might signify a new physical effect. Of course the only way to uncover this possibility is by an appropriate first-principles calculation.

AUTHOR INFORMATION

Corresponding Authors

Joel M. Bowman − *Cherry L. Emerson Center for Scientific Computation and Department of Chemistry, Emory University, Atlanta, Georgia 30322, United States;* orcid.org/0000-0001-9692-2672; Email: jmbowma@emory.edu

Paul Houston − *Department of Chemistry and Chemical Biology, Cornell University, Ithaca, New York 14853, United States; Department of Chemistry and Biochemistry, Georgia Institute of Technology, Atlanta, Georgia 30332, United States;* orcid.org/0000-0003-2566-9539; Email: plh2@cornell.edu

Author

Apurba Nandi − *Cherry L. Emerson Center for Scientific Computation and Department of Chemistry, Emory University, Atlanta, Georgia 30322, United States;* orcid.org/0000-0002-6191-5584

Complete contact information is available at: https://pubs.acs.org/10.1021/acs.jpca.0c04348

Notes

The authors declare no competing financial interest.

ACKNOWLEDGMENTS

We thank Professor Marta Menendez for sending data in ref 29 and also for sending TST rate constants for the $^3A'$ and $^3A''$ PESs. J.M.B. thanks Professor Bill Green for sending his Python code to evaluate the Eckart transmission coefficient. That was used to check our Python code. J.M.B. also thanks NASA (Grant 80NSSC20K0360) for financial support.

REFERENCES

(1) Eckart, C. The Penetration of a Potential Barrier by Electrons. *Phys. Rev.* **1930**, *35*, 1303−1309.

(2) Johnston, H. S.; Rapp, D. Large Tunnelling Corrections in Chemical Reaction Rates.[1] II. *J. Am. Chem. Soc.* **1961**, *83*, 1−9.

(3) Johnston, H. S.; Heicklen, J. Tunneling Corrections for Unsymmetrical Eckart Potential Energy Barriers. *J. Phys. Chem.* **1962**, *66*, 532−533.

(4) Barker, J. R.; Nguyen, T. L.; Stanton, J. F. Kinetic Isotope Effects for Cl + CH_4 → HCl + CH_3 Calculated Using Ab Initio Semiclassical Transition State Theory. *J. Phys. Chem. A* **2012**, *116*, 6408−19.

(5) Allison, T. C.; Truhlar, D. G. TESTING THE ACCURACY OF PRACTICAL SEMICLASSICAL METHODS: VARIATIONAL TRANSITION STATE THEORY WITH OPTIMIZED MULTI-DIMENSIONAL TUNNELING. *Modern Methods for Multidimensional Dynamics Computations in Chemistry* **1998**, 618−712.

(6) Schatz, G. C.; Kuppermann, A. Quantum Mechanical Reactive Scattering for Three-Dimensional Atom Plus Diatom Systems. II. Accurate Cross Sections for H+H_2. *J. Chem. Phys.* **1976**, *65*, 4668−4692.

(7) Bowman, J. M. Reduced Dimensionality Theories of Quantum Reactive Scattering. *Adv. Chem. Phys.* **2007**, *61*, 115−167.

(8) Bowman, J. M.; Wagner, A. F. Reduced Dimensionality Theories of Quantum Reactive Scattering: Applications to Mu+H2, H+H2,

https://dx.doi.org/10.1021/acs.jpca.0c04348
J. Phys. Chem. A 2020, 124, 5746−5755

O(3P)+H2, D2 and HD. *The Theory of Chemical Reaction Dynamics* **1986**, *170*, 47−76.
(9) Bowman, J. M. Reduced Dimensionality Theory of Quantum Reactive Scattering. *J. Phys. Chem.* **1991**, *95*, 4960−4968.
(10) Althorpe, S. C.; Clary, D. C. Quantum Scattering Calculations on Chemical Reactions. *Annu. Rev. Phys. Chem.* **2003**, *54*, 493−529.
(11) von Horsten, H. F.; Banks, S. T.; Clary, D. C. An Efficient Route to Thermal Rate Constants in Reduced Dimensional Quantum Scattering Simulations: Applications to the Abstraction of Hydrogen from Alkanes. *J. Chem. Phys.* **2011**, *135*, 094311.
(12) Marcus, R. A.; Coltrin, M. E. A New Tunneling Path for Reactions such as $H+H_2 \rightarrow H_2+H$. *J. Chem. Phys.* **1977**, *67*, 2609−2613.
(13) Miller, W. H. Semiclassical Limit of Quantum Mechanical Transition State Theory for Nonseparable Systems. *J. Chem. Phys.* **1975**, *62*, 1899−1906.
(14) Zhao, Y.; Yamamoto, T.; Miller, W. H. Path Integral Calculation of Thermal Rate Constants within the Quantum Instanton Approximation: Application to the $H+CH_4 \rightarrow H_2+CH_3$ Hydrogen Abstraction Reaction in Full Cartesian Space. *J. Chem. Phys.* **2004**, *120*, 3100−3107.
(15) Miller, W. H.; Hernandez, R.; Handy, N. C.; Jayatilaka, D.; Willetts, A. Ab initio Calculation of Anharmonic Constants for a Transition State, with Application to Semiclassical Transition State Tunneling Probabilities. *Chem. Phys. Lett.* **1990**, *172*, 62−68.
(16) Hernandez, R.; Miller, W. H. Semiclassical Transition State Theory. A New Perspective. *Chem. Phys. Lett.* **1993**, *214*, 129−136.
(17) Nguyen, T. L.; Stanton, J. F.; Barker, J. R. Ab initio Reaction Rate Constants Computed using Semiclassical Transition-State Theory: $HO + H_2 \rightarrow H_2O + H$ and Isotopologues. *J. Phys. Chem. A* **2011**, *115*, 5118−26.
(18) Wagner, A. F. Improved Multidimensional Semiclassical Tunneling Theory. *J. Phys. Chem. A* **2013**, *117*, 13089−100.
(19) Clary, D. C. Spiers Memorial Lecture Introductory Lecture: Quantum Dynamics of Chemical Reactions. *Faraday Discuss.* **2018**, *212*, 9−32.
(20) Craig, I. R.; Manolopoulos, D. E. Chemical Reaction Rates from Ring Polymer Molecular Dynamics. *J. Chem. Phys.* **2005**, *122*, 084106.
(21) Suleimanov, Y. V.; de Tudela, R. P.; Jambrina, P. G.; Castillo, J. F.; Sáez-Rábanos, V.; Manolopoulos, D. E.; Aoiz, F. J. A Ring Polymer Molecular Dynamics Study of the Isotopologues of the $H+H_2$ Reaction. *Phys. Chem. Chem. Phys.* **2013**, *15*, 3655−3665.
(22) Richardson, J. O. Perspective: Ring-Polymer Instanton Theory. *J. Chem. Phys.* **2018**, *148*, 200901.
(23) Miller, W. H.; Schwartz, S. D.; Tromp, J. W. Quantum Mechanical Rate Constants for Bimolecular Reactions. *J. Chem. Phys.* **1983**, *79*, 4889−4898.
(24) Wu, T.; Werner, H.-J.; Manthe, U. First-Principles Theory for the $H + CH_4 \rightarrow H_2 + CH_3$ Reaction. *Science* **2004**, *306*, 2227−2229.
(25) Welsch, R.; Manthe, U. Reaction Dynamics with the Multi-Layer Multi-Configurational Time-Dependent Hartree Approach: $H + CH_4 \rightarrow H_2 + CH_3$ Rate Constants for Different Potentials. *J. Chem. Phys.* **2012**, *137*, 244106.
(26) Suleimanov, Y. V.; Collepardo-Guevara, R.; Manolopoulos, D. E. Bimolecular Reaction Rates from Ring Polymer Molecular Dynamics: Application to $H + CH_4 \rightarrow H_2 + CH_3$. *J. Chem. Phys.* **2011**, *134*, 044131.
(27) Welsch, R. Rigorous Close-Coupling Quantum Dynamics Calculation of Thermal Rate Constants for the Water Formation Reaction of H_2 + OH on a High-Level PES. *J. Chem. Phys.* **2018**, *148*, 204304.
(28) Sun, P.; Zhang, S.; Chen, J.; Liu, S.; Zhang, D. H. Well Converged Quantum Rate Constants for the $H_2 + OH \rightarrow H_2O + H$ Reaction via Transition State Wave Packet. *J. Chem. Phys.* **2018**, *149*, 064303.
(29) Menendez, M.; Jambrina, P. G.; Zanchet, A.; Verdasco, E.; Suleimanov, Y. V.; Aoiz, F. J. New Stress Test for Ring Polymer Molecular Dynamics: Rate Coefficients of the $O(^3P)$ + HCl Reaction and Comparison with Quantum Mechanical and Quasiclassical Trajectory Results. *J. Phys. Chem. A* **2019**, *123*, 7920−7931.
(30) Houston, P. L.; Nandi, A.; Bowman, J. M. A Machine Learning Approach for Prediction of Rate Constants. *J. Phys. Chem. Lett.* **2019**, *10*, 5250−5258.
(31) Brown, R. L. A Method of Calculating Tunneling Corrections for Eckart Potential Barriers. *J. Res. Natl. Bur. Stand.* **1981**, *86*, 357−359.
(32) Rasmussen, C. E.; Williams, C. K. I. *Gaussian processes for machine learning*; The MIT Press: 2006.
(33) Vieira, D.; Krems, R. V. Rate Constants for Fine-structure Excitations in O−H Collisions with Error Bars Obtained by Machine Learning. *Astrophys. J.* **2017**, *835*, 255.
(34) Bartók, A. P.; Csányi, G. Gaussian Approximation Potentials: A Brief Tutorial Introduction. *Int. J. Quantum Chem.* **2015**, *115*, 1051−1057.
(35) Cui, J.; Krems, R. V. Efficient Non-Parametric Fitting of Potential Energy Surfaces for Polyatomic Molecules with Gaussian Processes. *J. Phys. B: At., Mol. Opt. Phys.* **2016**, *49*, 224001.
(36) Pedregosa, F.; Varoquaux, G.; Gramfort, A.; Michel, V.; Thirion, B.; Grisel, O.; Blondel, M.; Prettenhofer, P.; Weiss, R.; Dubourg, V.; Vanderplas, J.; Passos, A.; Cournapeau, D.; Brucher, M.; Perrot, M.; Duchesnay, E. Scikit-learn: Machine Learning in Python. *J. Mach. Learn. Res.* **2011**, *12*, 2825−2830.
(37) Koizumi, H.; Schatz, G. C.; Gordon, M. S. An Analytical Representation of the Lowest Potential Energy Surface for the Reaction $O(^3P) + HCl\ (X^1\Sigma^+) \rightarrow OH(X^2\Pi) + Cl(^2P)$. *J. Chem. Phys.* **1991**, *95*, 6421−6428.
(38) Thompson, W. H.; Miller, W. H. On the "Direct" Calculation of Thermal Rate Constants. II. The Flux-flux Autocorrelation Function with Absorbing Potentials, with Application to the O +HCl → OH+Cl Reaction. *J. Chem. Phys.* **1997**, *106*, 142−150.
(39) Tolstikhin, O. I.; Nakamura, H. Hyperspherical Elliptic Coordinates for the Theory of Light Atom Transfer Reactions in Atom-diatom Collisions. *J. Chem. Phys.* **1998**, *108*, 8899−8921.
(40) Poirier, B. Quantum Reactive Scattering for Three-body Systems via Optimized Preconditioning, as Applied to the O+HCl Reaction. *J. Chem. Phys.* **1998**, *108*, 5216−5224.
(41) Aoiz, F. J.; Bañares, L.; Castillo, J. F.; Menéndez, M.; Verdasco, J. E. Quantum Mechanical and Quasi-classical Rate Constant Calculations for the $O(^3P)$+HCl → OH+Cl Reaction. *Phys. Chem. Chem. Phys.* **1999**, *1*, 1149−1158.
(42) Matzkies, F.; Manthe, U. Combined Iterative Diagonalization and Statistical Sampling in Accurate Reaction Rate Calculations: Rotational Effects in O+HCl → OH+Cl. *J. Chem. Phys.* **2000**, *112*, 130−136.
(43) Skokov, S.; Zou, S.; Bowman, J. M.; Allison, T. C.; Truhlar, D. G.; Lin, Y.; Ramachandran, B.; Garrett, B. C.; Lynch, B. J. Thermal and State-Selected Rate Coefficients for the O(3P) + HCl Reaction and New Calculations of the Barrier Height and Width. *J. Phys. Chem. A* **2001**, *105*, 2298−2307.
(44) Xie, T.; Wang, D.; Bowman, J. M.; Manolopoulos, D. E. Resonances in the $O(^3P)$+HCl Reaction Due to van der Waals Minima. *J. Chem. Phys.* **2002**, *116*, 7461−7467.
(45) Xie, T.; Bowman, J. M.; Peterson, K. A.; Ramachandran, B. Quantum Calculations of the Rate Constant for the $O(^3P)$+HCl Reaction on New Ab initio A′ and A″ Surfaces. *J. Chem. Phys.* **2003**, *119*, 9601−9608.
(46) Menendez, M. Personal communication.
(47) Bowman, J. M. Enhancement of Tunneling Due to Resonances in Pre-barrier Wells in Chemical Reactions. *Chem. Phys.* **2005**, *308*, 255−257.
(48) *GPR for rate constants*. https://scholarblogs.emory.edu/bowman/gpr-for-rate-constants/.

https://dx.doi.org/10.1021/acs.jpca.0c04348
J. Phys. Chem. A 2020, 124, 5746−5755